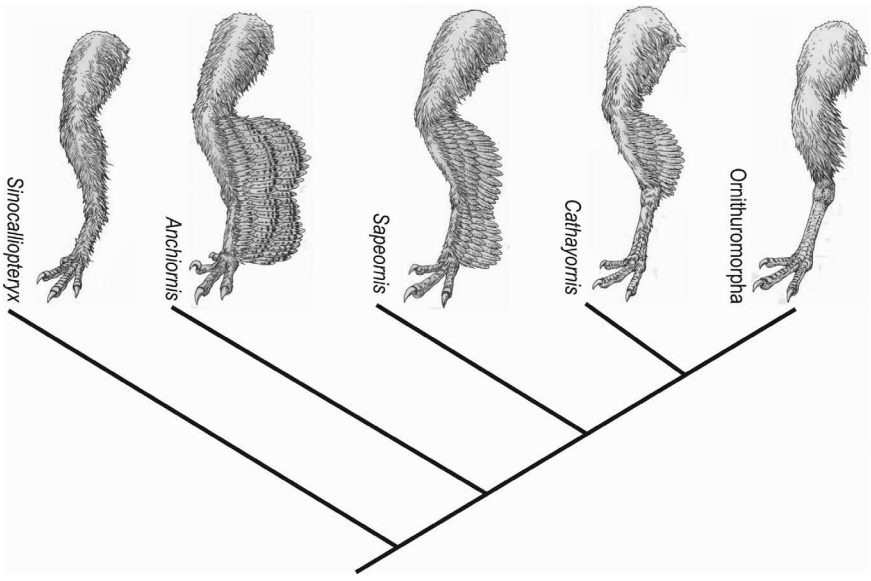

Fig. 4. Evolution of leg feathers in coelurosaurian dinosaurs. Four major stages in the evolution of integumentary structures on the hindlimb are represented by the compsognathid *Sinocalliopteryx* (short filamentous feathers covering legs, including feet); the basal deinonychosaurian *Anchiornis* and the basal avialan *Sapeornis* (large pennaceous feathers on legs, including feet, forming a winglike structure); the enantiornithine *Cathayornis* (large femoral and crural feathers forming a reduced winglike structure); and ornithuromorphs (small femoral and crural feathers and featherless feet).

References and Notes

1. X. Xu *et al.*, *Nature* **421**, 335 (2003).
2. X. Xu, F.-C. Zhang, *Naturwissenschaften* **92**, 173 (2005).
3. D. Y. Hu, L.-H. Hou, L. J. Zhang, X. Xu, *Nature* **461**, 640 (2009).
4. X. Xu, H. You, K. Du, F. Han, *Nature* **475**, 465 (2011).
5. D. E. Alexander, E. Gong, L. D. Martin, D. A. Burnham, A. R. Falk, *Proc. Natl. Acad. Sci. U.S.A.* **107**, 2972 (2010).
6. S. Chatterjee, R. J. Templin, *Proc. Natl. Acad. Sci. U.S.A.* **104**, 1576 (2007).
7. R. O. Prum, *Nature* **421**, 323 (2003).
8. F. C. Zhang, Z. H. Zhou, *Nature* **431**, 925 (2004).
9. N. R. Longrich, *Paleobiology* **32**, 417 (2006).
10. K. Padian, *Bioscience* **53**, 451 (2003).
11. K. Padian, K. P. Dial, *Nature* **438**, E3, discussion E3 (2005).
12. See the supplementary materials on *Science* Online.
13. Z. Zhou, P. M. Barrett, J. Hilton, *Nature* **421**, 807 (2003).
14. Z. H. Zhou, F. C. Zhang, *Can. J. Earth Sci.* **40**, 731 (2003).
15. L. H. Hou, C. M. Chuong, A. Yang, X. L. Zeng, J. F. Hou, *Fossil Birds of China* (Yunnan Science and Technology Press, Kunming, China, 2003).
16. L. M. Chiappe, S.-A. Ji, Q. Ji, M. A. Norell, *Bull. Am. Mus. Nat. Hist.* **242**, 1 (1999).
17. Z. Zhou, F. C. Zhang, *Proc. Natl. Acad. Sci. U.S.A.* **102**, 18998 (2005).
18. H. L. You *et al.*, *Science* **312**, 1640 (2006).
19. F. C. Zhang, Z. H. Zhou, *Nature* **438**, E4 (2005).
20. X. Xu, *Deinonychosaurian Fossils from the Jehol Group of Western Liaoning and the Coelurosaurian Evolution* (Chinese Academy of Sciences, Beijing, China, 2002).
21. M. Norell *et al.*, *Nature* **416**, 36 (2002).
22. Q. Ji, M. A. Norell, K.-Q. Gao, S.-A. Ji, D. Ren, *Nature* **410**, 1084 (2001).
23. X. Xu *et al.*, *Chin. Sci. Bull.* **54**, 430 (2009).
24. M. A. R. Koehl, D. Evangelista, K. Yang, *Integr. Comp. Biol.* **56**, 1002 (2011).
25. J. Hall, H. J. Habib, M. Hone, L. Chiappe, *J. Vertebr. Paleontol.* **32**, 105B (2012).
26. C. W. Beebe, *Zool. Sci. Contrib. N.Y. Zool. Soc.* **2**, 39 (1915).
27. S. A. Ji, Q. Ji, J. C. Lu, C. X. Yuan, *Acta Geol. Sin.* **81**, 8 (2007).
28. X. Xu *et al.*, *Nature* **484**, 92 (2012).
29. X. Xu, Z.-L. Tang, X.-L. Wang, *Nature* **399**, 350 (1999).
30. Q. Ji, P. J. Currie, M. A. Norell, S.-A. Ji, *Nature* **393**, 753 (1998).
31. A. M. Lucas, P. R. Stettenheim, *Avian Anatomy: Integument* (U.S. Department of Agriculture, Washington, DC, 1972).
32. L. Kelso, E. H. Kelso, *Auk* **53**, 51 (1936).
33. W. P. Maddison, D. R. Maddison (2011), http://mesquiteproject.org.
34. M. Logan, *Development* **130**, 6401 (2003).
35. R. H. Sawyer, L. W. Knapp, *J. Exp. Zool.* **298B**, 57 (2003).
36. M. P. Harris, B. L. Linkhart, J. F. Fallon, *Dev. Dyn.* **231**, 22 (2004).
37. R. B. Widelitz, T.-X. Jiang, J.-F. Lu, C. M. Chuong, *Dev. Biol.* **219**, 98 (2000).
38. F. Prin, D. Dhouailly, *Int. J. Dev. Biol.* **48**, 137 (2004).
39. S. M. Gatesy, K. P. Dial, *Evolution* **50**, 331 (1996).

Acknowledgments: Support for this research was provided by the National Natural Sciences Foundation of China (NNSFC grant nos. 41172016, 41120124002, and 41125008), the National Basic Research Program of China (grant no. 2012CB821900), and the Chinese Academy of Sciences (grant no. KZCX2-EW-105). We thank K. Padian and C. Sullivan for critical comments; C.-M. Chuong and T. Stidham for discussions; R. Li and H. Zang for illustrations; X. Ding for preparation of some of the specimens; and O. Rauhut, M. Koebl-Ebert, and M. Roeper for access to *Archaeopteryx* specimens.

Supplementary Materials

www.sciencemag.org/cgi/content/full/339/6125/1309/DC1
Supplementary Text
Figs. S1 to S10
Tables S1 to S3
References (*40*–*60*)

13 August 2012; accepted 20 December 2012
10.1126/science.1228753

Adaptive Evolution of Multiple Traits Through Multiple Mutations at a Single Gene

Catherine R. Linnen,[1]* Yu-Ping Poh,[2,4,6] Brant K. Peterson,[2,3] Rowan D. H. Barrett,[2] Joanna G. Larson,[2] Jeffrey D. Jensen,[5,6] Hopi E. Hoekstra[2,3]*

The identification of precise mutations is required for a complete understanding of the underlying molecular and evolutionary mechanisms driving adaptive phenotypic change. Using plasticine models in the field, we show that the light coat color of deer mice that recently colonized the light-colored soil of the Nebraska Sand Hills provides a strong selective advantage against visually hunting predators. Color variation in an admixed population suggests that this light Sand Hills phenotype is composed of multiple traits. We identified distinct regions within the *Agouti* locus associated with each color trait and found that only haplotypes associated with light trait values have evidence of selection. Thus, local adaptation is the result of independent selection on many mutations within a single locus, each with a specific effect on an adaptive phenotype, thereby minimizing pleiotropic consequences.

Darwin believed that adaptation occurred through "slight successive variations" (*1*). Fisher later elaborated on this idea by proposing the geometric model of adaptation (*2*), which assumes that most mutations are pleiotropic and therefore that mutations of small phenotypic effect are more likely than those of large effect to bring a population closer to its fitness optimum. To test Fisher's model, we must identify individual mutations and assess both their phenotypic effects and their degree of pleiotropy. Although recent years have seen considerable progress in identifying loci or genes underlying adaptive phenotypes [reviewed in (*3*, *4*)], few have genetically dissected these loci to the level of individual mutations [but see (*5*–*8*)], and none have examined multiple traits at this level

of resolution. Thus, it remains unclear whether genes that contribute to complex phenotypes (i.e., those composed of multiple traits) tend to do so through single pleiotropic mutations or multiple mutations with independent effects.

Deer mice (*Peromyscus maniculatus*) living on the light-colored soils of the Nebraska Sand Hills, a massive dune field formed only 8000 to 15,000 years ago (*9*), are lighter than conspecifics living on the surrounding dark soils (*10*, *11*) (Fig. 1, A and B). To test the hypothesis that this light pelage is an adaptation for crypsis, we measured attack rates on light and dark plasticine mouse models (Fig. 1C) at multiple Sand Hills sites [following (*12*); also see (*13*)]. We found that conspicuous, dark models were attacked significantly more often than cryptic, light models ($P < 0.05$) (Fig. 1D). Together with previous experiments using avian predators and live mice (*14*), these results strongly suggest that the overall light color of Sand Hills mice is a recent adaptation driven, at least in part, by visually hunting predators.

The light dorsal fur of Sand Hills mice is largely caused by a change at the *Agouti* locus. Specifically, a derived cis-acting increase in the duration and magnitude of *Agouti* expression during hair growth leads to a concomitant increase in the width of light pigmented bands on individual hairs (*11*). However, upon closer inspection of phenotypic variation, we found that Sand Hills and wild-type mice differ in multiple pigmentation traits that together give rise to the overall cryptic appearance of the Sand Hills mice (Fig. 2A). In addition to having a significantly lighter dorsum (one-tailed *t* test; $N = 10$ lab-reared mice; $P = 8.2 \times 10^{-4}$), Sand Hills mice also have a lighter ventrum, an upward shift in the dorsal-ventral (d-v) boundary, and a less pronounced tail stripe compared with the ancestral form (one-tailed *t* tests; $N = 10$ mice; ventral color: $P = 3.9 \times 10^{-5}$; d-v boundary: $P = 1.4 \times 10^{-4}$; tail stripe: $P = 5.5 \times 10^{-7}$). Because these derived light-color traits are all associated with *Agouti* in laboratory strains, they could be explained by either a single pleiotropic mutation of large effect or multiple mutations of smaller, more modular effect in this locus.

To distinguish between these alternatives, we collected phenotypic (color and color pattern) and genotypic data from 91 wild-caught mice from a phenotypically diverse population located near the edge of the Sand Hills. We measured three color traits derived from a principal component analysis (PCA) of spectrophotometric data (dorsal hue, dorsal brightness, and ventral color) (table S1) and two color pattern traits (d-v boundary and tail stripe). Phenotypes in this wild population were largely independent (R^2 range: 0.04 to 0.27) (table S2). In fact, several trait pairs lacked a significant correlation in spite of a large sample size (e.g., dorsal hue and d-v boundary, $P = 0.69$, $N = 91$ mice). These data suggest that these pigment traits are likely under independent genetic control.

To dissect the molecular basis of these traits, we combined a targeted enrichment strategy with next-generation sequencing [following (*15*)] to generate polymorphism data for ~2100 unlinked regions averaging 1.5 thousand base pairs (kbp) in length and a 185-kbp region containing *Agouti* and all known regulatory elements (Fig. 2B) (*16*). Using a genetic PCA on genome-wide polymorphism data (*13*), we identified four significant genetic principal components, none of which were associated with color (table S3). These data indicate that light and dark mice interbreed freely, and genetic structure is not associated with color variation in this population. Next, we examined linkage disequilibrium (LD) across *Agouti* (fig. S1) and found that the 95th percentile of r^2 falls below 0.4 within 3 kbp (fig. S2). The extremely low level of LD is considerably less than reported for wild populations of *Mus musculus* (*17*); however, this is not surprising given the large effective population size we estimated for *P. maniculatus* ($N_e > 50{,}000$ mice) (*13*). Together, these data suggest that there has been sufficient recombination for fine-scale mapping color traits within *Agouti*.

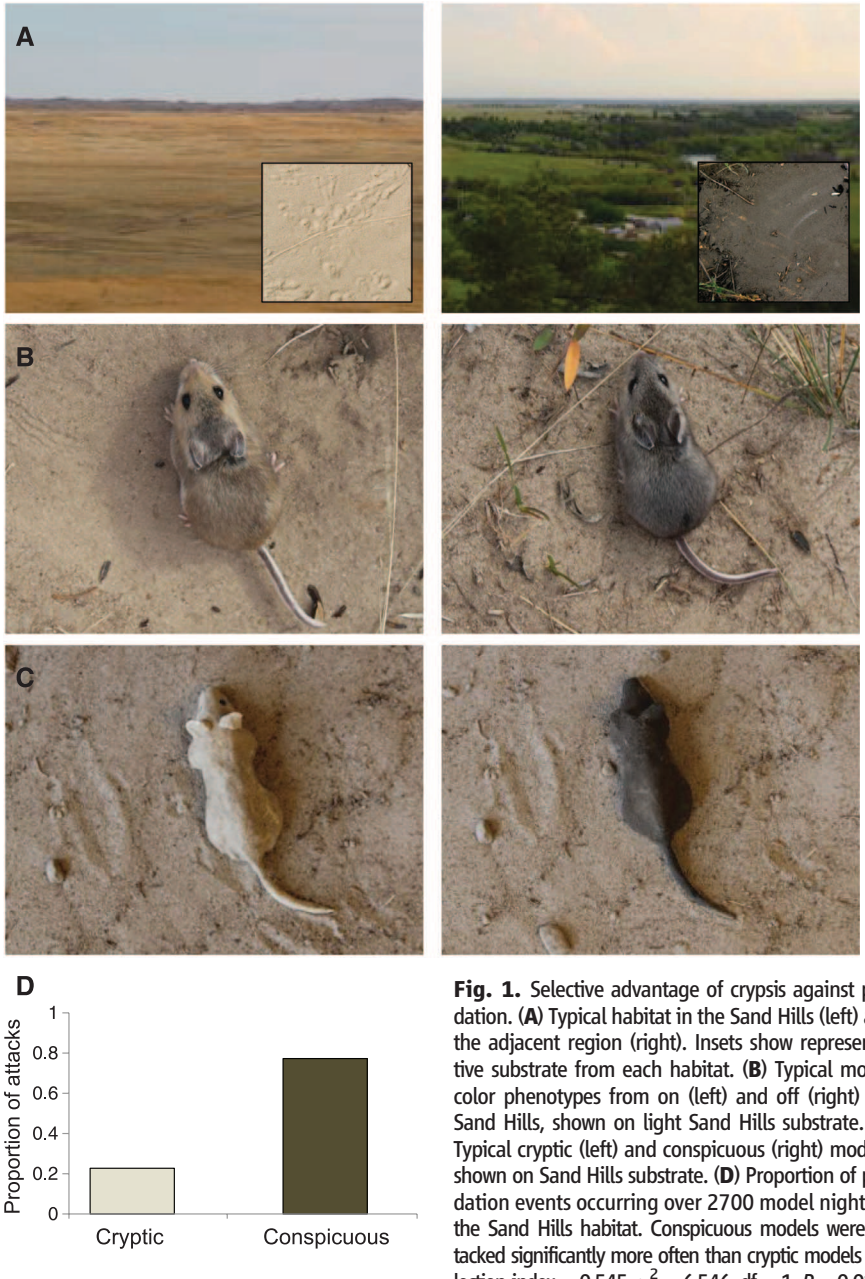

Fig. 1. Selective advantage of crypsis against predation. (**A**) Typical habitat in the Sand Hills (left) and the adjacent region (right). Insets show representative substrate from each habitat. (**B**) Typical mouse color phenotypes from on (left) and off (right) the Sand Hills, shown on light Sand Hills substrate. (**C**) Typical cryptic (left) and conspicuous (right) models, shown on Sand Hills substrate. (**D**) Proportion of predation events occurring over 2700 model nights in the Sand Hills habitat. Conspicuous models were attacked significantly more often than cryptic models (selection index = 0.545, $\chi^2 = 6.546$, df = 1, $P = 0.011$).

[1]Department of Biology, University of Kentucky, 200A Thomas Hunt Morgan Building, Lexington, KY 40506, USA. [2]Department of Organismic and Evolutionary Biology, the Museum of Comparative Zoology, Harvard University, 26 Oxford Street, Cambridge, MA 02138, USA. [3]Department of Molecular and Cellular Biology, Harvard University, 26 Oxford Street, Cambridge, MA 02138, USA. [4]Program in Bioinformatics and Integrative Biology, University of Massachusetts Medical School, Worcester, MA, USA. [5]School of Life Science, Ecole Polytechnique Fédérale de Lausanne (EPFL), Lausanne, Switzerland. [6]Swiss Institute of Bioinformatics (SIB), Lausanne, Switzerland.

*To whom correspondence should be addressed. E-mail: catherine.linnen@uky.edu (C.R.L.); hoekstra@oeb.harvard.edu (H.E.H.)

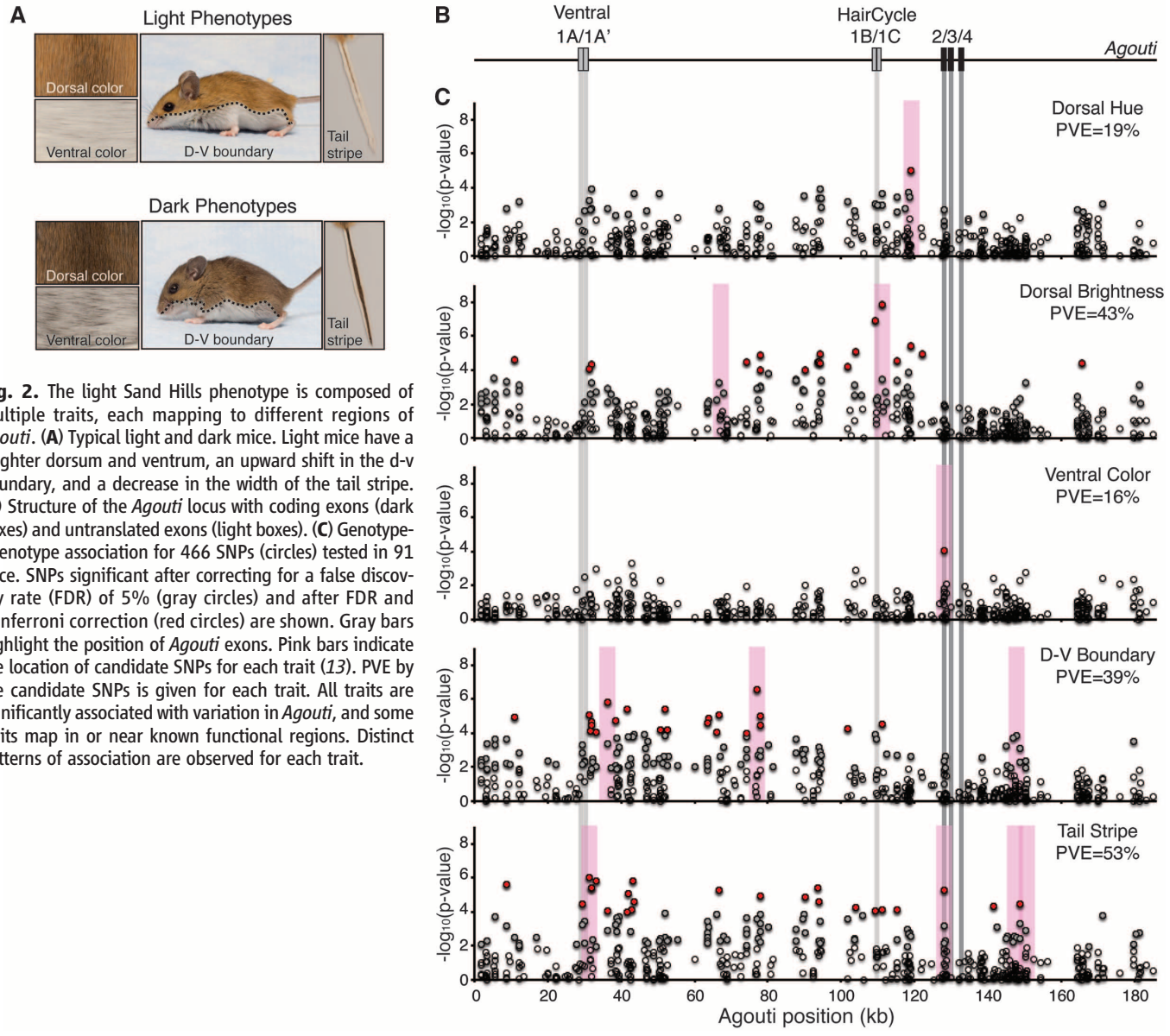

Fig. 2. The light Sand Hills phenotype is composed of multiple traits, each mapping to different regions of *Agouti*. (**A**) Typical light and dark mice. Light mice have a brighter dorsum and ventrum, an upward shift in the d-v boundary, and a decrease in the width of the tail stripe. (**B**) Structure of the *Agouti* locus with coding exons (dark boxes) and untranslated exons (light boxes). (**C**) Genotype-phenotype association for 466 SNPs (circles) tested in 91 mice. SNPs significant after correcting for a false discovery rate (FDR) of 5% (gray circles) and after FDR and Bonferroni correction (red circles) are shown. Gray bars highlight the position of *Agouti* exons. Pink bars indicate the location of candidate SNPs for each trait (*13*). PVE by the candidate SNPs is given for each trait. All traits are significantly associated with variation in *Agouti*, and some traits map in or near known functional regions. Distinct patterns of association are observed for each trait.

To identify associations between these *Agouti* genotypes and color phenotypes, we used both single-SNP (single-nucleotide polymorphism) linear regressions and a multiple-SNP Bayesian approach (*13*, *18*). Based on these analyses, we found each of the five color traits was statistically associated with a unique set of SNPs that together explained 16 to 53% of the variation (Fig. 2C and fig. S3). There was one exception: a serine deletion (ΔSer) in exon 2 was associated with both ventral color ($P = 8.5 \times 10^{-5}$) and tail stripe ($P = 5.4 \times 10^{-6}$). Notably, no single set of polymorphisms could account for variation across all five traits (table S4). These findings demonstrate that there are multiple mutations that contribute to different aspects of the light Sand Hills phenotype.

Additionally, several traits were associated with SNPs that fell in or near regions of known functional importance. Two *Agouti* isoforms under the control of different promoters have been identified: The ventral isoform containing noncoding exons 1A/1A′ is restricted to the ventral dermis and is required to establish the dorsal-ventral boundary during embryogenesis, and the hair-cycle-specific isoform containing noncoding exons 1B/1C is expressed in adults during hair growth and leads to the formation of light, pheomelanin bands on individual hairs (*19*, *20*) (Fig. 2B). In our data, the d-v boundary and tail stripe traits mapped near the ventral promoter; dorsal brightness mapped near the hair-cycle promoter; and ventral color and tail stripe mapped to a deletion (ΔSer) in exon 2, which is a conserved residue located in a protein domain that interacts with another pigment protein Attractin (*21*) (Fig. 2C, fig. S3, and table S5). These results suggest that multiple molecular mechanisms—including both protein-coding and cis-regulatory changes—are involved in color adaptation in these Sand Hills mice.

Having identified multiple regions contributing to coat-color lightness, we tested for positive selection on *Agouti* and these specific polymorphisms. We used *dadi* (*22*) to estimate a demographic model and parameters for our ecotonal population. We found evidence suggesting that the population experienced a recent (~2900 years ago) bottleneck, in which the population was reduced to 0.4% of its original size, followed by an exponential recovery to ~65% of its original size. Using this demographic model and the Sweepfinder framework (*23*), we evaluated patterns of selection in both the entire data set (i.e., all sampled individuals) and 10 polarized data sets (i.e., in which light and dark haplotypes are defined by the genotype at the candidate SNP of interest), following (*11*, *13*, *24*). We identified two regions with evidence of selection acting on all mice collected from this location, independent of coat color (Fig. 3A). By comparison, in polarized data

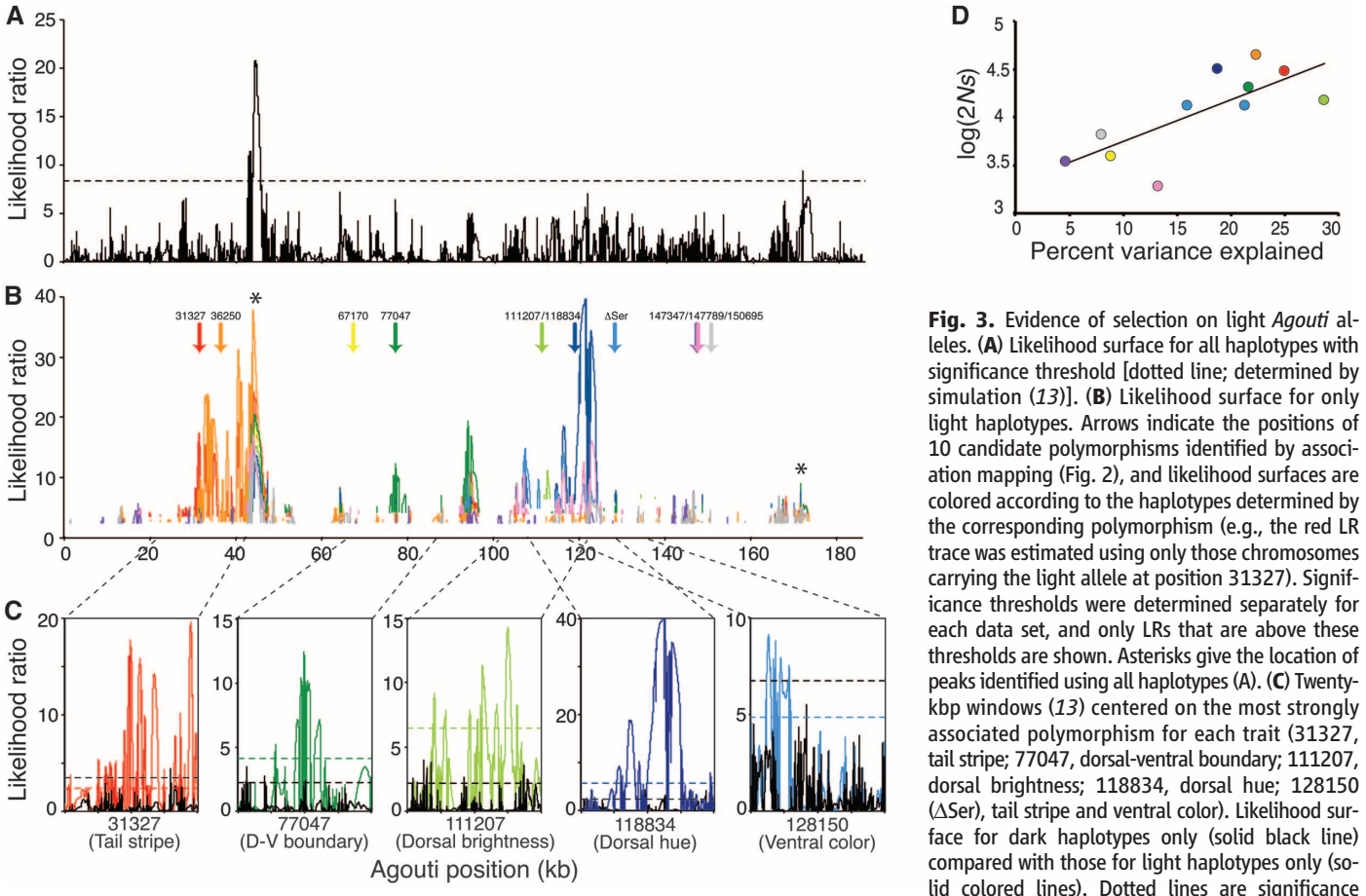

Fig. 3. Evidence of selection on light *Agouti* alleles. (**A**) Likelihood surface for all haplotypes with significance threshold [dotted line; determined by simulation (*13*)]. (**B**) Likelihood surface for only light haplotypes. Arrows indicate the positions of 10 candidate polymorphisms identified by association mapping (Fig. 2), and likelihood surfaces are colored according to the haplotypes determined by the corresponding polymorphism (e.g., the red LR trace was estimated using only those chromosomes carrying the light allele at position 31327). Significance thresholds were determined separately for each data set, and only LRs that are above these thresholds are shown. Asterisks give the location of peaks identified using all haplotypes (A). (**C**) Twenty-kbp windows (*13*) centered on the most strongly associated polymorphism for each trait (31327, tail stripe; 77047, dorsal-ventral boundary; 111207, dorsal brightness; 118834, dorsal hue; 128150 (ΔSer), tail stripe and ventral color). Likelihood surface for dark haplotypes only (solid black line) compared with those for light haplotypes only (solid colored lines). Dotted lines are significance thresholds (black, dark only; colored, light only). **(D)** Strength of selection (*s*) is significantly correlated with PVE (R^2 = 0.56; Spearman's rho = 0.76; P = 0.0071). Color of each SNP as in (B).

Table 1. Selection on candidate regions identified using association mapping. PVE (R^2) after controlling for population structure is given for each polymorphism. Asterisk denotes the ΔSer in exon 2 that was associated with more than one trait. These SNPs were then used to classify haplotypes as "light" or "dark" depending on observed phenotype-genotype correlations; selection analyses were performed separately on light and dark haplotypes. The distance (in base pairs) to the nearest site with a significant LR and the number of significant sites within a 20-kbp window surrounding the polarizing site are given for both light and dark alleles. Selection coefficients [*s*; assuming N_e = 53,080 mice (*13*)] and average 2*Ns* are also provided. Selection coefficients vary among traits; within each trait, SNPs with higher PVE have higher *s*.

Candidate	Trait	PVE	Light allele				Dark allele			
			Distance	No. of sites	2*Ns*	*s*	Distance	No. of sites	2*Ns*	*s*
118834	Dorsal hue	18.8	2393	2769	32,038	0.302	2607	207	2348	0.022
67170	Dorsal brightness	8.9	641	91	3926	0.037	2935	170	3977	0.038
111207	Dorsal brightness	28.7	881	588	15,296	0.144	1532	161	3047	0.029
ΔSer*	Ventral color	16	4084	802	13,366	0.126	41831	0	3121	0.029
36250	d-v boundary	22.4	7	5476	44,598	0.420	2880	1237	7122	0.067
77047	d-v boundary	21.7	0	1446	20,855	0.197	76	102	4959	0.047
147789	d-v boundary	13.3	2657	26	1921	0.018	741	369	2262	0.021
31327	Tail stripe	25	0	2986	30,324	0.286	3898	155	3992	0.038
ΔSer*	Tail stripe	21.3	4084	802	13,366	0.126	41,831	0	3121	0.029
147347	Tail stripe	4.7	733	1360	3447	0.033	24	176	1254	0.012
150695	Tail stripe	8	318	803	6730	0.063	1980	244	2399	0.023

sets, we found significant likelihood peaks clustered around the location of the polarizing SNPs (Fig. 3B and Table 1), consistent with recent selection acting on, or near, color-associated SNPs. Using one-tailed Wilcoxon signed-rank tests for our 10 candidate SNPs, we found that, compared with the dark-associated alleles (Fig. 3C and Table 1), light-associated alleles have a significantly better correspondence between the location of the polarizing SNP and the nearest significant likelihood-ratio (LR) peak (P = 0.037), a significantly greater number of sites surrounding the polarizing SNP that reject neutrality (P = 0.0063), and a significantly higher selection coefficient (P = 0.0063). Also, these differences are robust to choice of window size (tables S6 and S7). These observations are consistent with multiple targets of selection among the light, but not dark, alleles of *Agouti*.

We next estimated the strength of selection acting on these light-associated SNPs, using a maximum likelihood approach implemented in Sweepfinder (*13*, *23*). Selection coefficients (*s*) ranged from 0.018 to 0.42 (Table 1), suggesting very strong selection in some cases. Selection strength varied as a function of both color trait and phenotypic effect size: We observed especially strong selection on SNPs associated with dorsal hue, dorsal-ventral boundary, and tail stripe (Table 1) and a positive correlation between the percent variation explained (PVE) and *s* across all light-associated SNPs (Spearman's Rank correlation = 0.76, P = 0.0071, one-tailed) (Fig. 3D). Moreover, within each trait, we see a perfect rank correlation between PVE and *s* (e.g., for tail stripe

associated SNPs Spearman's rho = 1, $P = 0$, $N = 4$ SNPs). Thus, for each candidate SNP, the stronger its effect on color phenotype, the stronger the estimate of selection strength, suggesting that these mutations likely have minimal pleiotropic consequences. These results, when combined with results from the clay model experiment, the extensive recombination across this region, and the association mapping study, all support a scenario in which multiple independent *Agouti* mutations—each contributing to a distinct trait associated with the light phenotype—have been selected for cryptic coloration on the Sand Hills.

Although it has been suggested that pigmentation is an unusually simple trait (*25*), when deconstructed, we find both phenotypic and genetic complexity. The light pigmentation of the Sand Hills mice is composed of several genetically independent traits, and we find that mutations associated with each show clear signatures of selection. These results imply that each color trait, from dorsal color to tail stripe, independently affects fitness. We also demonstrate how a large-effect locus can fractionate into many small- to moderate-effect mutations. Moreover, although the gene *Agouti* has widespread effects on pigmentation, measurable pleiotropic effects are largely absent at the mutational level, serving as a reminder that, although it is commonplace to discuss the degree of pleiotropy of individual genes, it is individual mutations, not genes, that bring a population closer to its phenotypic optimum. Together, our results suggest that small, minimally pleiotropic mutations—even those occurring within a single gene—may provide a rapid route to adaptation along multiple phenotypic axes.

References and Notes

1. C. Darwin, *On the Origin of Species by Means of Natural Selection, or the Preservation of Favoured Races in the Struggle for Life* (John Murray, London, 1859).
2. R. A. Fisher, *The Genetical Theory of Natural Selection* (Oxford Univ. Press, Oxford, 1930).
3. N. J. Nadeau, C. D. Jiggins, *Trends Genet.* **26**, 484 (2010).
4. J. Stapley *et al.*, *Trends Ecol. Evol.* **25**, 705 (2010).
5. H. E. Hoekstra, R. J. Hirschmann, R. A. Bundey, P. A. Insel, J. P. Crossland, *Science* **313**, 101 (2006).
6. M. Rebeiz, J. E. Pool, V. A. Kassner, C. F. Aquadro, S. B. Carroll, *Science* **326**, 1663 (2009).
7. N. Frankel *et al.*, *Nature* **474**, 598 (2011).
8. K. V. S. K. Prasad *et al.*, *Science* **337**, 1081 (2012).
9. D. B. Loope, J. Swinehart, *Great Plains Res.* **10**, 5 (2000).
10. L. R. Dice, *Contrib. Lab. Vertebr. Genet. Univ. Mich.* **15**, 1 (1941).
11. C. R. Linnen, E. P. Kingsley, J. D. Jensen, H. E. Hoekstra, *Science* **325**, 1095 (2009).
12. S. N. Vignieri, J. G. Larson, H. E. Hoekstra, *Evolution* **64**, 2153 (2010).
13. Materials and methods are available as supplementary materials on *Science* online.
14. L. R. Dice, *Contrib. Lab. Vertebr. Biol. Univ. Mich.* **34**, 1 (1947).
15. V. S. Domingues *et al.*, *Evolution* **66**, 3209 (2012).
16. E. P. Kingsley, M. Manceau, C. D. Wiley, H. E. Hoekstra, *PLoS ONE* **4**, e6435 (2009).
17. C. C. Laurie *et al.*, *PLoS Genet.* **3**, e144 (2007).
18. Y. Guan, M. Stephens, *Ann. Appl. Stat.* **5**, 1780 (2011).
19. S. J. Bultman *et al.*, *Genes Dev.* **8**, 481 (1994).
20. H. Vrieling, D. M. J. Duhl, S. E. Millar, K. A. Miller, G. S. Barsh, *Proc. Natl. Acad. Sci. U.S.A.* **91**, 5667 (1994).
21. P. J. Jackson *et al.*, *Chem. Biol.* **13**, 1297 (2006).
22. R. N. Gutenkunst, R. D. Hernandez, S. H. Williamson, C. D. Bustamante, *PLoS Genet.* **5**, e1000695 (2009).
23. R. Nielsen *et al.*, *Genome Res.* **15**, 1566 (2005).
24. C. D. Meiklejohn, Y. Kim, D. L. Hartl, J. Parsch, *Genetics* **168**, 265 (2004).
25. M. V. Rockman, *Evolution* **66**, 1 (2012).

Acknowledgments: We thank K. Duryea and G. Goncalves for laboratory assistance; J. Chupasko, E. Kay, E. Kingsley, M. Manceau, and J. Weber for field assistance; J. Demboski and the Denver Museum of Nature and Science for logistical support; and J. Chupasko for curation assistance. C.R.L. was supported by a Ruth Kirschstein National Research Service Award from NIH; B.K.P. by a Jane Coffins Child Postdoctoral Fellowship; J.D.J. and Y-P.P. by grants from the Swiss National Science Foundation, the European Research Council, and Defense Advanced Research Projects Agency; R.D.H.B. by a Natural Sciences and Engineering Research Council of Canada Banting Postdoctoral Fellowship and a Foundational Questions in Evolutionary Biology Postdoctoral Fellowship. Laboratory and fieldwork was funded by Putnam Expedition Grants from the MCZ Museum of Comparative Zoology (MCZ), the Swiss National Science Foundation, Harvard University, and the National Science Foundation (DEB-0749958 to H.E.H.). *P. maniculatus* were collected under the Nebraska Game and Parks Commission Scientific and Educational Permit 901, and voucher specimens were deposited in the MCZ's Mammal Department. Sequence data were deposited in the NCBI Short Read Archive (accession no. SRP017939). **Author contributions:** C.R.L., J.D.J., and H.E.H. designed the project; C.R.L. conducted field work; B.K.P. designed capture array and short-read analysis pipeline; C.R.L. and B.K.P. collected genomic data; C.R.L. and J.G.L. collected phenotypic data; C.R.L., Y.-P.P., and B.K.P. analyzed the data; R.D.H.B. and C.R.L. conducted the plasticine model experiment; and C.R.L. and H.E.H. wrote the paper with input from the other authors.

Supplementary Materials

www.sciencemag.org/cgi/content/full/339/6125/1312/DC1
Materials and Methods
Figs. S1 to S3
Tables S1 to S9
References (*26*–*47*)

27 November 2012; accepted 4 February 2013
10.1126/science.1233213

Circadian Control of Chloroplast Transcription by a Nuclear-Encoded Timing Signal

Zeenat B. Noordally,[1] Kenyu Ishii,[2] Kelly A. Atkins,[3] Sarah J. Wetherill,[3] Jelena Kusakina,[4] Eleanor J. Walton,[3] Maiko Kato,[2] Miyuki Azuma,[5] Kan Tanaka,[6] Mitsumasa Hanaoka,[2] Antony N. Dodd[4]*

Circadian timekeeping in plants increases photosynthesis and productivity. There are circadian oscillations in the abundance of many chloroplast-encoded transcripts, but it is not known how the circadian clock regulates chloroplast transcription or the photosynthetic apparatus. We show that, in *Arabidopsis*, nuclear-encoded SIGMA FACTOR5 (SIG5) controls circadian rhythms of transcription of several chloroplast genes, revealing one pathway by which the nuclear-encoded circadian oscillator controls rhythms of chloroplast gene expression. We also show that SIG5 mediates the circadian gating of light input to a chloroplast-encoded gene. We have identified an evolutionarily conserved mechanism that communicates circadian timing information between organelles with distinct genetic systems and have established a new level of integration between eukaryotic circadian clocks and organelles of endosymbiotic origin.

Circadian clocks coordinate biological systems with the Earth's day-night cycles. Because circadian regulation increases photosynthesis and productivity (*1*), we wished to understand how the circadian clock controls the timing of events within chloroplasts. Chloroplasts contain small cyanobacteria-derived genomes that encode essential components of the photosynthetic apparatus. Interrogation of four circadian transcript profiles from *Arabidopsis thaliana* indicates that 62 (70%) of the 88 protein-coding genes encoded by the chloroplast genome can be circadian regulated (spreadsheet S1) (*2*). Chloroplast genes are transcribed by either nuclear-encoded plastid RNA polymerase (NEP) or plastid-encoded plastid RNA polymerase (PEP). PEP comprises five core plastid-encoded subunits and requires one of several nuclear-encoded sigma factors of prokaryotic ancestry to confer promoter specificity to PEP (*3*). The *Arabidopsis* genome encodes six sigma factors (*3*), and all sigma factors can be circadian regulated, depending on experimental conditions (spreadsheet S1). In *Arabidopsis*, some sigma factors are required for gene expression during chloroplast biogenesis [e.g., SIGMA FACTOR2 (SIG2) and SIG6], and others adjust the photosynthetic apparatus during steady-state photosynthesis (e.g., SIG1 and SIG5) (*4*–*7*). We hypothesized that sigma factors might communicate circadian timing information from the nucleus to chloroplasts, if there are oscillations in

[1]SynthSys, University of Edinburgh, C H Waddington Building, Mayfield Road, Edinburgh EH9 3JD, UK. [2]Graduate School of Horticulture, Chiba University, 648 Matsudo, Matsudo, Chiba 271-8510, Japan. [3]Department of Biology, University of York, York YO10 5DD, UK. [4]School of Biological Sciences, University of Bristol, Bristol BS8 1UG, UK. [5]Institute of Molecular and Cellular Biosciences, The University of Tokyo, 1-1-1 Yayoi, Bunkyo-ku, Tokyo 113-0032, Japan. [6]Chemical Resources Laboratory, Tokyo Institute of Technology, 4259 Nagatsuta, Midori-ku, Yokohama 226-8503, Japan.

*To whom correspondence should be addressed. E-mail: antony.dodd@bristol.ac.uk